Mismatch Corrections for Electro-Optic Sampling Systems*

Dylan F. Williams, Paul D. Hale, Tracy S. Clement, and Juanita M. Morgan
National Institute of Standards and Technology
325 Broadway, Boulder, CO 80305
e-mail: dylan, hale, clementt, morgan@boulder.nist.gov

***Abstract*-** We develop and apply frequency-domain mismatch corrections to a temporal electro-optic sampling system. We use these corrections to characterize the magnitude and phase of electrical sources that are physically far removed from the point at which the electro-optic sampling system measures voltage waveforms. We demonstrate the technique by determining the power spectrum of a photoreceiver's optical impulse response.

Introduction

In this paper we develop frequency-domain mismatch corrections for temporal electro-optic sampling systems. These mismatch corrections allow us to determine Thévenin and Norton equivalent circuits for electrical sources, as well as the voltage they would deliver to an ideal 50 Ω load. The technique can be applied to sources that are far removed from the point at which the electro-optic sampling system measures voltage waveforms.

Figure 1 shows a schematic diagram of our electro-optic sampling system, which is similar to those described in [1]. The laser generates a train of roughly 100 fs pulses in an open collimated beam. We split the laser output into two beams: an "excitation" beam, and a "sampling" beam. We chop the excitation beam, launch it into an optical fiber, and then use it to excite the photoreceiver that we wish to characterize. The photoreciever has a optical

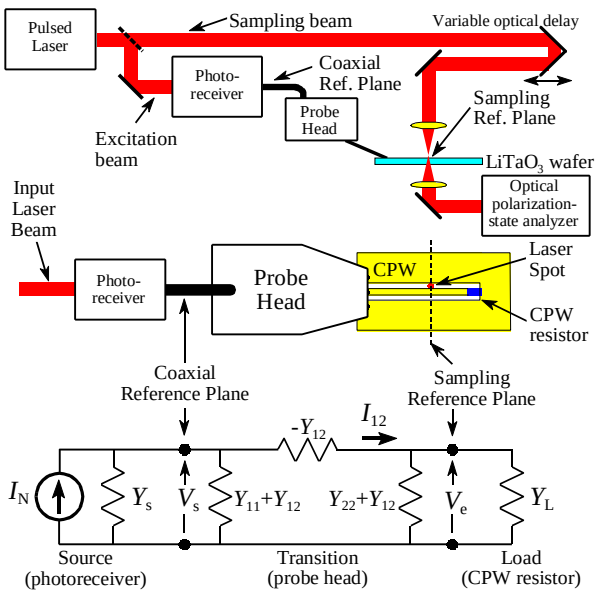

Fig. 1. A schematic diagram of our electro-optic sampling system (top), a top-view schematic (center), and an electrical equivalent circuit (bottom). The photoreceiver generates a train of electrical impulses at the coaxial reference plane when it is excited by optical pulses at its input. These electrical impulses propagate through the probe head to the CPW on the electro-optic $LiTaO_3$ substrate, where they are sampled by the sampling beam.

fiber input and a coaxial electrical output, and contained a photodiode, biasing circuit, and electrical matching network. When illuminated by the optical excitation beam, the photoreceiver creates a series of electrical impulses at its coaxial output. The pulses in the optical excitation beam are so short compared to the response time of the photoreceiver, that the electrical signals generated by the

photoreceiver are, for practical purposes, equal to the receiver's electrical impulse response, which we would like to measure.

The electrical impulses generated by the photoreceiver propagate through the probe head and down to a coplanar waveguide (CPW) fabricated on an electro-optic y-cut $LiTaO_3$ wafer. The direction of propagation in the CPW is parallel to the x-axis of the $LiTaO_3$, and the CPW is terminated with an open circuit or a planar resistor.

The probe head, CPW, and CPW termination in the electro-optic sampling system distort the electrical impulses emanating from the photoreceiver. The sampling beam then reconstructs the distorted electrical waveform in the CPW fabricated on the $LiTaO_3$ wafer. We pass this sampling beam through a variable optical delay, polarize it, and then focus it through a small gap in our coplanar line, as illustrated in Fig. 1. The electric field between the CPW conductors changes the polarization of the optical beam passing through the wafer. By changing the delay of the sampling beam, we incrementally adjust the relative time at which the optical sampling pulse reaches the surface of the wafer, and are thus able to trace out the electrical waveform on the wafer as it evolves with time.

Figure 2 shows two sampled voltage waveforms in the CPW on our $LiTaO_3$ wafer we measured with our electro-optic sampling system. Both waveforms were generated by the same photoreceiver under the same bias and excitation conditions. However, one of the waveforms was measured in a CPW terminated with an open circuit, while the other was measured in a CPW terminated with a planar resistor with a 34.8 Ω DC resistance.

The figure shows that the CPW resistor quickly, although not entirely, dampens the

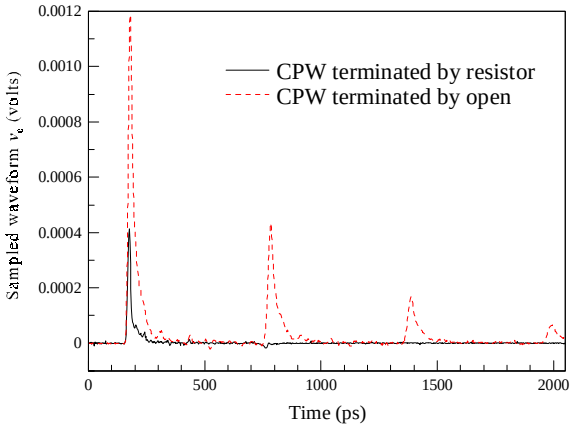

Fig. 2. Two waveforms measured by our electro-optic sampling system. The solid line corresponds to a measurement with the CPW terminated by a 34.8 Ω resistor, and the dashed line corresponds to a measurement with the CPW terminated by an open circuit. Except for these terminations, all of the conditions in the experiment were identical.

multiple reflections with a roughly 500 ps period in the setup. This reflection corresponds to signals making round-trips between the photoreceiver and the CPW resistor. The first small negative reflection off of this CPW resistor, which occurs approximately 10 ps after the main pulse, most likely decreases and sharpens the impulse slightly over what we would see if the CPW were terminated with a perfect 50 Ω resistor. The first positive reflection off of the open circuit, on the other hand, increases the amplitude of the main pulse greatly and broadens it.

None of the components of the system have real frequency-independent impedances. In addition, the probe head, its connection to the CPW, and the CPW itself, which has a complex and frequency-dependent characteristic impedance, distort both pulses. This makes it impossible to choose a perfect terminating resistor. In what follows, we will show how to use frequency-domain measurements to correct for the effects of the CPW load, probe heads, and connection to the CPW in the measurements. These data yield the power

spectrum of the electrical response of the photoreceiver to a fast optical input, a quantity that is independent of the probe head, CPW, and the CPW load.

Mismatch Corrections

Our electro-optic sampling system measures the voltage $v_e(t)$ at the sampling reference plane in Fig. 1. To correct for the probe head, its connection to the CPW, and the CPW termination, we first performed a coaxial frequency-domain short-open-load-thru (SOLT) vector-network-analyzer calibration at the coaxial reference plane in the system, and then measured the reflection coefficient $\Gamma_s(f)$ of the photoreceiver over the frequency range 0 to 40 GHz.

We then performed a second-tier multiline thru-reflect-line (TRL) vector-network-analyzer calibration [2] directly at the sampling reference plane in the CPW, setting the reference impedance to 50 Ω using the method of [3]. This calibration is based on direct broadband measurements of the traveling waves in the CPW, and avoids errors inherent in on-wafer SOLT calibrations. We measured the reflection coefficient $\Gamma_L(f)$ of the CPW terminations with this calibration, and determined the scattering parameters $S_{ij}(f)$ of the probe head, which were equal to the "error boxes" determined by the second-tier TRL calibration.

Once we determined the electrical reflection coefficients Γ_s of the photoreceiver and Γ_L of the CPW load, and the scattering parameters S_{ij} of the probe head, in the frequency domain using our vector network analyzer, we determined the admittances Y_s of the photoreceiver and Y_L of the CPW load, and the admittance parameters Y_{ij} of the probe head, using standard transformations. Finally, we constructed the equivalent circuit shown in Fig. 1, which is based on these measured quantities.

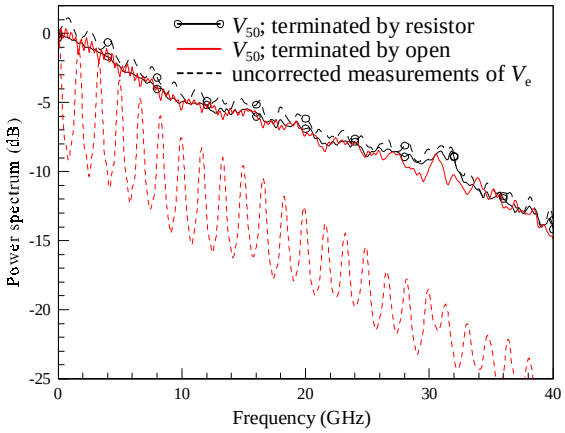

Fig. 3. A comparison of the corrected power spectrums of V_{50} for the two waveforms shown in Fig. 2. The uncorrected spectrums of V_e are shown in dashed lines. The curves are normalized to 0 dB at DC.

To determine the photoreceiver's Norton equivalent current I_N in the frequency domain, we first obtained the Fourier transform $V_e(f)$ of the time-domain waveform $v_e(t)$ measured by the electro-optic sampling system. Then, using Kirchhoff's laws, we calculated the internal current $I_{12}(f)$ from

$$I_{12} = V_e(Y_L + Y_{22} + Y_{12}), \qquad \textbf{(1)}$$

the voltage V_s at the coaxial reference plane from

$$V_s = I_{12} Y_2^{-1}, \qquad \textbf{(2)}$$

and the photoreceiver's Norton equivalent current I_N from

$$I_N = V_s(Y_s + Y_{11} + Y_{12} + Y_2), \qquad \textbf{(3)}$$

where

$$Y_2 \equiv \left[-Y_{12}^{-1} + (Y_{22} + Y_{12} + Y_L)^{-1}\right]^{-1}. \qquad \textbf{(4)}$$

Here I_N is the current that the photoreceiver would supply to a perfect short circuit at the coaxial reference plane when excited by a short optical impulse.

From I_N we can obtain the Thévenin equivalent voltage $V_T(f)$ that the photoreceiver would generate across a perfect open circuit at

the coaxial reference plane from

$$V_T \equiv \frac{I_N}{Y_s} = I_N Z_s \qquad \textbf{(5)}$$

where $Z_s \equiv Y_s^{-1}$ is the photoreceiver's electrical input impedance. We obtain the voltage $V_{50}(f)$ the photoreceiver would generate across a perfect 50 Ω load at the coaxial reference plane from

$$V_{50} = V_T \frac{50}{50 + Z_s}. \qquad \textbf{(6)}$$

Figure 3 compares the power spectra of V_e, the uncorrected waveform measured by the electro-optic sampling system, and V_{50}, the voltage the photoreceiver would deliver to a perfect 50 Ω coaxial load, corresponding to the two time-domain waveforms shown in Fig. 2. The corrections not only reduce the "ripple" in the measurements, but they also correct rigorously for the attenuation and distortion of the probe heads, and for the broadening and narrowing of the main pulse caused by the two different CPW terminations.

Preliminary Comparison to Power-Sensor Calibrated Oscilloscope Measurements

The solid line in Fig. 4 shows the power spectrum of V_{50} for our photoreceiver as measured with our electro-optic sampling system. We noted that acoustic vibrations in our electro-optic sampling system introduced low-frequency offsets in the measurements, so we normalized this measurement such that a linear fit over the region 2 GHz to 8 GHz extrapolates to 0 dB at DC.

Figure 4 compares our electro-optic measurement of V_{50} to measurements we performed with a commercial sampling oscilloscope. We calibrated the oscilloscope with the "swept-sine" amplitude calibration [4]

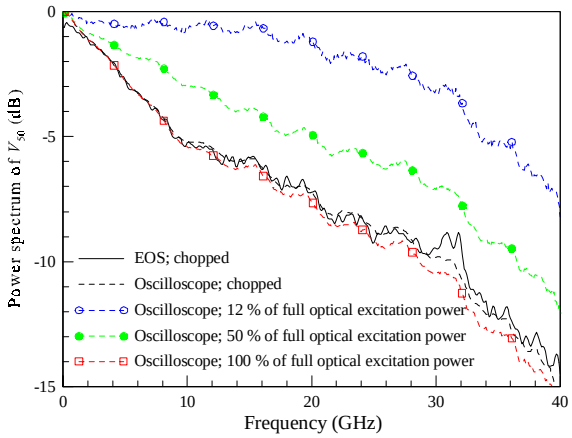

Fig. 4. Comparison of calibrated oscilloscope measurements at different optical input power levels to a corrected electro-optic-sampling-system measurement of the power spectrum of the impulse response of the photoreceiver. We normalized the EOS spectrum to extrapolate to 0 dB at DC.

as implemented in [5], and [6]. The oscilloscope calibration incorporates mismatch and drift corrections, and a power-sensor correction to calibrate the oscilloscope's amplitude response. We also normalized the oscilloscope measurements to extrapolate to 0 dB at DC.

The dashed lines in Fig. 4 show that our photoreciever's impulse response depends on the power of the optical pulses in the excitation beam. Since we chopped the excitation beam, the nonlinear response of our photoreceiver to its optical input complicated our comparison.

We used a mechanical chopper in our electro-optic sampling system to improve our signal to noise ratio. This chopper interrupts the excitation beam with a set of spinning blades. However, the chopper does not instantly turn on and off the optical excitation beam used to excite the photoreceiver. Rather, as the chopper blades rotate, it takes some time to fully block or let pass the optical excitation beam. This means that we were not always either fully blocking the excitation beam, or exciting the photoreceiver with the full power available from the excitation beam: over some part of the

chopper cycle, we excited the photoreceiver with a partially blocked excitation beam. Since, at least some of the time, we were actually exciting the photoreciever with a partially blocked beam, we do not expect the response we measure with our electro-optic sampling system to correspond exactly to the photoreceiver's response at a 100% power level.

To make a better comparison, we used our oscilloscope to average 3000 waveforms from the detector while its excitation beam was being chopped. This measurement is labeled "oscilloscope; chopped" in Fig. 4, and does agree well with the measurement we performed with our electro-optic sampling system, except at a narrow band of frequencies near 30 GHz.

Conclusion

We described electrical mismatch corrections for electro-optic sampling systems. The corrections allow the magnitude and phase response of a source far removed from the measurement reference plane to be accurately characterized. While in our case this source was connectorized, this same scheme could be used to simply translate the measurement reference plane down the CPW in which we made the electrical measurements.

Our comparisons to calibrated oscilloscope measurements were hampered by nonlinearity in our photoreceiver, the finite switching speed of the chopper, and acoustic noise generated by the chopper. We expect that we will be able to obtain better comparisons of photoreceiver response to calibrated oscilloscope measurements with linear photoreceivers and by improving our optical chopping system.

References

[1] B.H. Kolner and D.M. Bloom, "Electrooptic sampling in GaAs integrated circuits," *IEEE Jour. Quantum Electron.*, vol. QE-22, no. 1, pp. 79-93, Jan. 1986.

[2] R.B. Marks, "A Multiline Method of Network Analyzer Calibration," *IEEE Trans. Microwave Theory Tech.*, vol. 39, no. 7, pp. 1205-1215, July 1991.

[3] R.B. Marks and D.F. Williams, "Characteristic Impedance Determination using Propagation Constant Measurement," *IEEE Microwave Guided Wave Lett.*, vol. 1, no. 6, pp. 141-143, June 1991.

[4] J. Verspecht and K. Rush, "Individual characterization of broadband sampling oscilloscopes with a nose-to-nose calibration procedure," *IEEE Trans. Instrum. Meas.*, vol. 43, no. 2, pp. 347-354, April 1994.

[5] P.D. Hale, T.S. Clement, K.C. Coakley, C.M. Wang, D.C. DeGroot, and A.P. Verdoni, "Estimating the magnitude and phase response of a 50 GHz sampling oscilloscope using the 'nose-to-nose' method," *55th ARFTG Conference Digest*, June 2000.

[6] D. C. DeGroot and P. D. Hale, "Analysis of interconnection networks and mismatch in the nose-to-nose calibration,"*55th ARFTG Conference Digest*, June 2000